



In-situ investigation of pressure effect on structural evolution and conductivity of Na₃SbS₄ superionic conductor



Hui Wang^{a,*}, Ming Yu^b, Yan Wang^c, Zhenxing Feng^c, Yingqi Wang^d, Xujie Lü^d, Jinlong Zhu^e, Yang Ren^f, Chengdu Liang^{g,**}

^a Mechanical Engineering Department, Conn Center for Renewable Energy Research, University of Louisville, Louisville, KY, 40292, United States

^b Department of Physics and Astronomy, University of Louisville, Louisville, KY, 40292, United States

^c School of Chemical, Biological, and Environmental Engineering, Oregon State University, Corvallis, OR, 97331, United States

^d Center for High Pressure Science and Technology Advanced Research (HPSTAR), Shanghai 201203, China

^e Center for High Pressure Science and Technology Advanced Research (HPSTAR), Beijing 100090, China

^f X-ray Science Division, Advanced Photon Source, Argonne National Laboratory, Lemont, IL 60439, United States

^g Zhejiang Provincial Key Laboratory of Advanced Chemical Engineering Manufacture Technology, College of Chemical and Biological Engineering, Zhejiang University, Hangzhou, 310027, China

HPSTAR
638-2018

HIGHLIGHTS

- Both theoretical calculation and *in-situ* high-pressure experiments are integrated.
- Na₃SbS₄ keeps tetragonal structure but show anisotropic compressibility.
- The ionic conductivity of Na₃SbS₄ increases to 1.6 mS cm⁻¹ after pressure treatment.
- Decreased grain boundary resistance contributes to the increase of conductivity.

ARTICLE INFO

Keywords:

Solid-state battery
Na-ion conductor
Na₃SbS₄
Pressure effect
Structure
Conductivity

ABSTRACT

Sulfide-based conductors are one class of the most promising solid electrolytes for next-generation of all-solid-state batteries due to their advantages on high ionic conductivity and favorable mechanical properties of easy densification. Besides new material chemistry to be explored, understanding the pressure effect on structure and property is equally important from both fundamental and practical considerations, as pressure is one way to tune the properties of such solid electrolytes. Here we report the pressure-driven structural evolution and conductivity change of Na₃SbS₄ solid electrolyte through the integration of molecular dynamics (MD) simulation and *in-situ* experiments. Theoretical calculation predicts that no phase transition happens to tetragonal Na₃SbS₄ under 10 GPa isotopically pressure. Synchrotron X-ray diffraction and Raman results confirm that Na₃SbS₄ keeps stable tetragonal structure but shows anisotropic compressibility along different directions. After pressure release, the ionic conductivity of Na₃SbS₄ increases by four folds to 1.6 mS cm⁻¹, which is resulted from the dramatic decrease of grain boundary resistance.

1. Introduction

Sulfide-based solid conductors have attracted much attention because they show high ionic conductivity and require much lower sintering temperature than oxide crystals [1–4]. Extensive efforts have been devoted on exploring new compositions and a lot of superionic conductors such as Li₁₀GeP₂S₁₂ [5,6], Li₇P₃S₁₁ [7,8], β-Li₃PS₄ [9,10], Na₃PS₄ [11–13], and Na₃SbS₄ [14,15] have been discovered. These

solid conductors have ionic conductivities of 0.1–10 mS cm⁻¹, almost comparable with that of organic liquid electrolyte used in conventional Li-ion batteries. Furthermore, the ionic conductivities of these sulfide-based solid conductors are closely related with their crystal structures [9,11,16–18]. Na₃PS₄ shows dramatic conductivity difference in tetragonal and cubic structures [11], and the similar trend happens on γ-phase and β-phase Li₃PS₄ [9]. Besides superior conductivity, sulfide-based solid electrolytes also have favorable mechanical property of easy

* Corresponding author.

** Corresponding author.

E-mail addresses: hui.wang.1@louisville.edu, whui583@gmail.com (H. Wang), cd_liang@hotmail.com (C. Liang).

densification by cold pressing [19,20]. $\text{Li}_2\text{S}\cdot\text{P}_2\text{S}_5$ solid electrolyte was reported to show exceed 90% relative density after loading a pressure of 350 MP [20], in contrast to oxide conductors that require sintering temperature over 1000 °C to achieve the same level of densification. Compared with “hard” oxide crystals, sulfide-based solid conductors are “soft” and this behavior benefits for all-solid-state battery construction.

However, the “soft” feature of sulfide solid conductors also raise a concern on their phase durability after cold pressing because pressure is a basic thermodynamic parameter that may cause the phase transition of solid materials. ZnS had been reported to transfer from zincblende (ZB) to rocksalt (RS) structure under pressure [21], BaS also experienced pressure-induced phase transition from rocksalt structure to cesium chloride structure [22]. Furthermore, it had been compared that sulfides usually need lower pressure to achieve phase transition than oxide conductors. Obvious examples such as Li_2O and Li_2S , the former one requires 50 GPa to realize cubic to orthorhombic structure change, while the later one achieves the same phase transition at 12 GPa [23,24]. Since pressure-induced phase transitions can either be permanent or reversible, *in-situ* characterization techniques such as XRD and Raman have been employed for many solid-state materials [25–27].

Sodium sulfide (Na_3SbS_4), a recent discovered solid conductor that shows excellent ionic conductivity of 1 mS cm^{-1} [28,29] and impressive chemical stability in ambient environment. This material recently has attracted much research interests [30,31], and is considered to be a strong solid electrolyte candidate. We previously reported that Na_3SbS_4 shows tetragonal phase at room temperature and transfer to cubic structure at elevated temperature (120–150 °C) [28]. Since the structural stability under pressure is important to achieve a reliable performance, we here integrated ab-initio molecular dynamics (MD) simulation and *in-situ* experiments, including synchrotron X-ray diffraction (XRD), Raman and electrochemical impedance spectroscopy (EIS) to study the pressure effects on structural evolution and conductivity change of Na_3SbS_4 . Theoretical calculation predicts that no phase transition happens to Na_3SbS_4 up to 10 GPa. Synchrotron XRD results confirm that Na_3SbS_4 keeps stable tetragonal structure but shows anisotropic compressibility along different directions. After pressure release, the ionic conductivity of Na_3SbS_4 increases to 1.6 mS cm^{-1} due to the dramatic decrease of grain boundary resistance.

2. Experiments and methodology

2.1. Theoretical calculation method

The overall computational calculations in this study was mainly carried out employing the density functional theory (DFT) [32,33] framework, as implemented in the Vienna Ab-initio Simulation Package (VASP) [34] and performed for the structure optimization, phase transition process under pressures, energy barrier and diffusion. The electron-ion interactions were described by the Projector Augmented Wave (PAW) [35], while electron exchange-correlation interactions were treated by the generalized gradient approximation (GGA) [36] in the scheme of Perdew Burke Ernzerhof (PBE) [37]. The structural relaxation was performed using Congregate-Gradient algorithm [38] implemented in VASP. The micro-canonical ensemble was used in the MD simulation and all the atoms in the unit cell are allowed to move freely during the simulations. An energy cutoff was set to be 280 eV for the plane wave basis in all calculations, and the criteria for the convergences of energy and force in relaxation processes were set to be 10^{-5} eV and 10^{-4} eV/\AA , respectively. A $1 \times 1 \times 1$ cubic/tetragonal primitive cell was chosen and the Brillouin zones (BZ) were sampled by $10 \times 10 \times 10$ k-point meshes generated in accordance with the Monkhorst-Pack scheme [39] in all calculations. Molecular dynamics (MD) simulation for compression was performed by introducing various strain in the tetragonal and cubic structures of Na_3SbS_4 .

2.2. Materials synthesis

Na_3SbS_4 sample was synthesized following our previous work [28]. Sodium thioantimonysulfide nanohydrate ($\text{Na}_3\text{SbS}_4 \cdot 9\text{H}_2\text{O}$) was heated step by step to 150 °C under vacuum and hold for 1 h. The hydrate water was removed to produce pure Na_3SbS_4 .

2.3. In-situ structural characterizations under pressure

The *in-situ* high-pressure angle-dispersive X-ray diffraction (ADXRD) and Raman experiments were carried out at High-Pressure Collaborative Access Team (HPCAT) at the Advanced Photon Source (APS), Argonne National Laboratory (ANL). We employed a symmetrical diamond anvil cell (DAC) to generate high pressure for synchronic XRD and Raman in this research (Figure S1). Na_3SbS_4 sample and two small ruby balls were loaded into the sample chamber with gaskets for sealing. Neon was used as the pressure-transmitting medium, and the pressures were determined by the ruby fluorescence method. For ADXRD experiment, a focused monochromatic X-ray beam about $5 \mu\text{m}$ in diameter (FWHM) with a wavelength of 0.4066 \AA was used for the diffraction experiments. The diffraction data were recorded by a MAR345 image plate, and then the two-dimensional (2D) images were integrated to one-dimensional (1D) patterns with the Fit2D program. High-pressure Raman spectra were measured by a Raman spectrometer with a 532.1 nm excitation laser at HPCAT.

2.4. Conductivity measurement under pressure

Electrochemical impedance spectra (EIS) measurements were conducted for Na_3SbS_4 solid electrolyte within a home-designed die set using a high-resolution electrochemical potentiostat (Biologic SP200). The frequency is between 5 MHz and 1 Hz at the amplitude 100 mV. Na_3SbS_4 sample was loaded in the home-designed die (with Al/C as blocking electrode on each side) with hydrolytic press to load pressure. The Nyquist plot shows a typical semicircle at a higher-frequency region that represents the bulk and grain boundary resistance of the electrolyte, and a spike at a lower-frequency region that represents the diffusion due to the blocking electrode. The resistance (R) intercept of the semicircle at the axis of Z' (Ω) was employed to determine the total ionic conductivity (σ) by the equation $\sigma = \frac{L}{R \cdot A}$, where A is the cross-area and L is the thickness of pellets.

3. Results and discussion

3.1. Theoretical simulation

Na_3SbS_4 is known to possess two crystal structures [15,28]: one is body-centered tetragonal structure with space group of P421C, and the other one is body-centered cubic structure with space group of I43m (Fig. 1A and B). In tetragonal Na_3SbS_4 framework, there are two main sites for Na atoms with Zigzag alignment, Na(1) in a NaS_6 distorted octahedron and Na(2) in a NaS_8 dodecahedron. The coordinates of three elements in two different structures are listed in Table S1 in terms of Wyckoff notation. The optimized lattice constants are $a = 7.2214 \text{ \AA}$ and $c = 7.3529 \text{ \AA}$ for the tetragonal phase, and $a = 7.228 \text{ \AA}$ for cubic phase, which are close to experimental values [15]. To determine more stable structure (tetragonal or cubic) under pressure, the cohesive energy per atom (defined as $E_{\text{cohesive}} = E_{\text{total}} - \sum_{i=\text{element}} N_i E_i^{\text{atom}}$) was calculated for both structures at different pressure (compression). At zero pressure, the tetragonal phase (-3.719 eV/atom and 380.02 \AA^3) has 5 meV lower on cohesive energy per atom than that in cubic phase (-3.714 eV/atom and 377.68 \AA^3), in good consistent with the experiment observation that the tetragonal phase is more stable structure compared to the cubic at ambient pressure. Fig. 1C compares the cohesive energies of tetragonal structure and cubic structure at different levels of compression (with different unit cell volumes). This

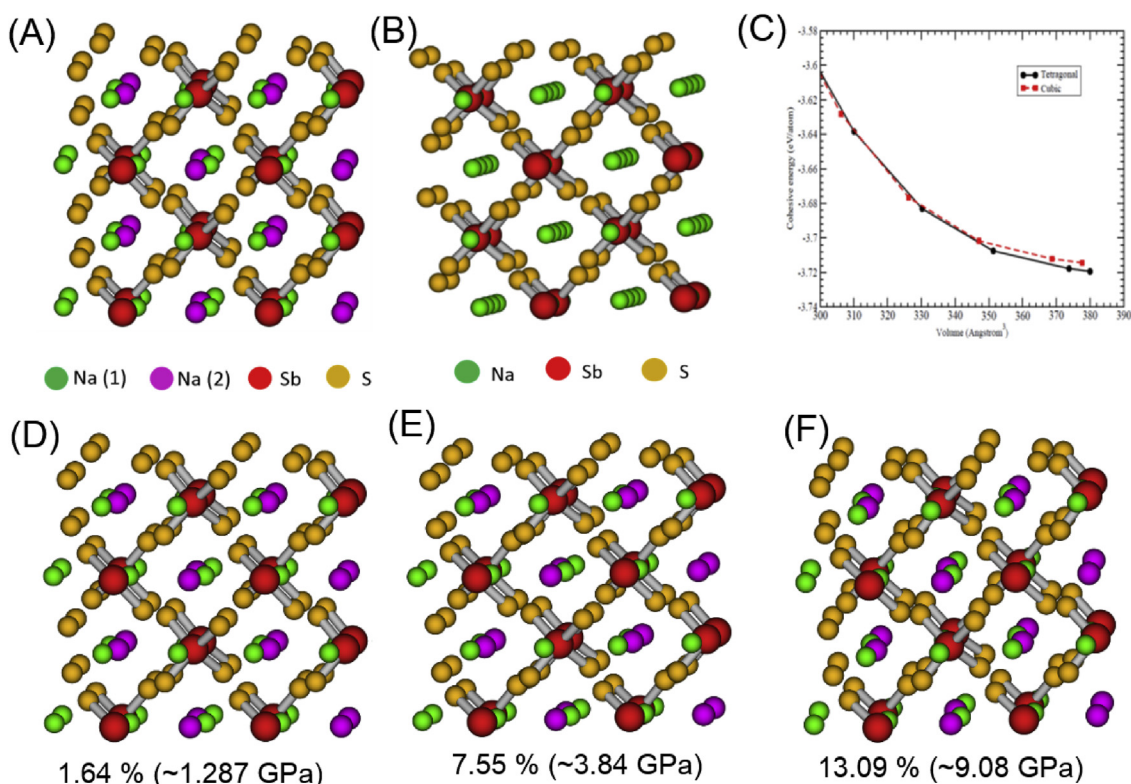


Fig. 1. Optimized crystal structure of Na_3SbS_4 (A) Tetragonal, (B) Cubic. (C) Comparison of Cohesive energy per atom of tetragonal and cubic structures as a function of unit cell volume under pressure. Optimized crystal structure of tetragonal Na_3SbS_4 under different levels of compression (D) 1.64% (1.28 GPa), (E) 7.55% (3.84 GPa), and (F) 13.09% (9.1 GPa) in volume.

comparison indicates that tetragonal structure of Na_3SbS_4 is more stable under pressure up to 10 GPa. It is possible to observe both tetragonal and cubic structures co-exist at even higher pressure. In addition, molecular dynamics (MD) simulation was performed by introducing various strain in the Na_3SbS_4 framework (Fig. 1D–F), which clearly show tetragonal behavior of zigzag aligned Na (1) and Na(2).

3.2. In-situ experiments on structural evolution under pressure

Although the temperature dependence of Na_3SbS_4 phase transition was previously reported [28], the *in-situ* structural evolution of Na_3SbS_4 under pressure was first investigated in this work through XRD and Raman. For the *in-situ* XRD, Na_3SbS_4 powder was loaded in a symmetrical DAC with ruby as the pressure-transmitting medium for high-pressure study. Fig. 2A shows the synchrotron XRD data and the refinement results, reflecting structure evolution of Na_3SbS_4 framework during compression. All XRD peaks of the Na_3SbS_4 sample can be assigned to the tetragonal phase, in which the characteristic diffraction peaks at $2\theta = 4.6^\circ, 7.9^\circ, 9.2^\circ, 12.1^\circ$, correspond to planes of (110), (211), (220) and (321), respectively. This observation is consistent with the theoretical calculation results. With an increase of pressure, diffraction peaks start to shift to larger 2θ values and the peak widths broadened gradually, which becomes more obvious when pressure is increased above 1.3 GPa due to the compression. From the refinements of XRD data that collect at different pressures, we plotted the unit cell volume versus pressure (P-V) curve (Fig. 2B) and the variation of lattice constant (a and c/a) of Na_3SbS_4 pressure (Fig. 2C). The a was found to decrease linear with pressure loading, and the c/a trends to increase from 1.018 at ambient pressure to 1.04 as pressure loaded at 2.0 GPa. The increased c/a ratio suggests that loading pressure increases the tetragonal distortion of Na_3SbS_4 framework, also further supports the theoretical calculation that tetragonal phase is more stable at high pressure than cubic. The variation of lattice constant (Fig. 2C and D)

indicates the anisotropic compressibility along different directions. The a was found to be more compressible than the c axis, which is the main contribution to the volume shrinkages.

In order to further characterize the pressure-induced local structure evolution, we collected Raman spectra of Na_3SbS_4 during compression–decompression cycles (Fig. 3A and B). At ambient pressure, Na_3SbS_4 shows strong characteristic peaks located at 410, 389 and 368 cm^{-1} , corresponding to asymmetric and symmetric stretching vibration of the SbS_4 group [40], respectively. When pressure is loaded, all the Raman peaks show a blue shift without the observation of new peaks until to 3.5 GPa (Fig. 3C), and then red shift back after releasing pressure (Fig. 3D). Raman spectra results also confirm that Na_3SbS_4 keeps the tetragonal phase stable under pressure, which is in good agreement with the XRD data and theoretical calculation. This finding indicates that the phase transition of Na_3SbS_4 is not sensitive to pressure, which is beneficial for this solid electrolyte to keep stable performance in practical applications.

3.3. Pressure effect on ionic conductivity

The ionic conductivity of Na_3SbS_4 as a function of pressure was investigated by measuring electrochemical impedance spectra (EIS). Fig. 4A shows the relationship between the loading pressure and the ionic conductivity of Na_3SbS_4 solid electrolyte during the first cycle of compression and decompression process. When pressure is loaded on Na_3SbS_4 , its conductivity rises quickly to 0.7 mS cm^{-1} at 0.4 GPa, then increases gradually to 1 mS cm^{-1} at 0.9 GPa and tends to be constant beyond. This behavior is similar with previous report on $\text{Li}_2\text{S-P}_2\text{S}_5$ glass solid electrolyte under pressure [20]. The Nyquist plots of Na_3SbS_4 under different pressure during compression and decompression process are shown in Fig. 4B. The typical impedance plot exhibits a semi-circular region at higher frequencies and a spike at lower frequencies, corresponding to the bulk/grain boundary resistance and diffusion

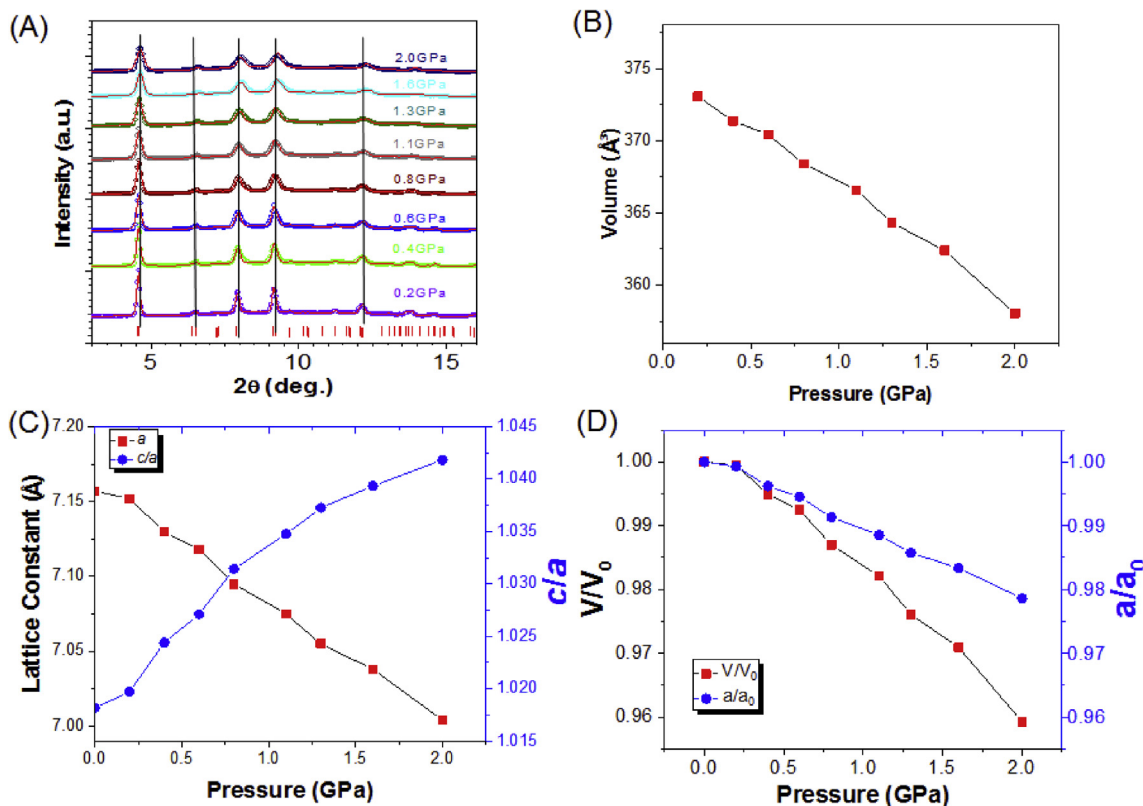


Fig. 2. (A) Synchrotron X-ray diffraction data and refinements of Na₃SbS₄ as a function of applied pressure, and pressure dependence of (B) unit cell volume, (C) lattice constant *a* and tetragonality *c/a*, (D) *V/V₀* and *a/a₀*.

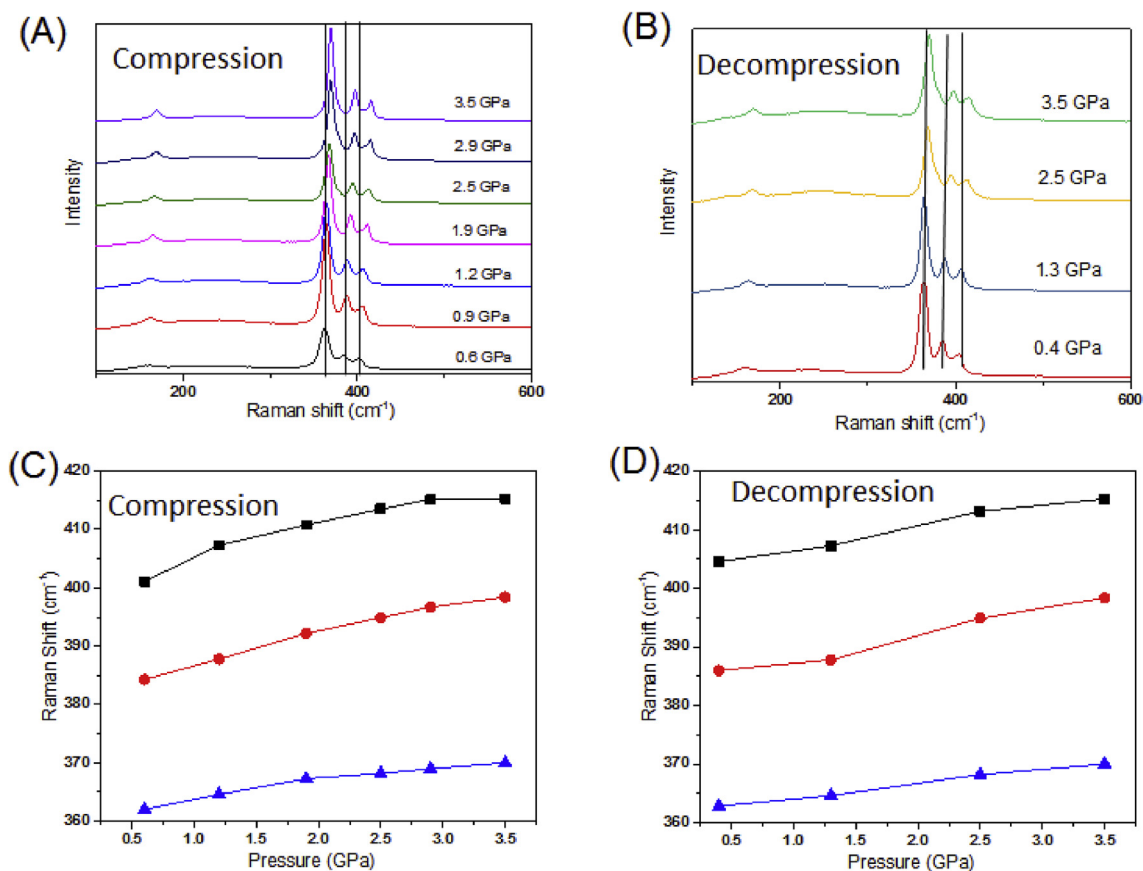


Fig. 3. Raman spectra of Na₃SbS₄ during (A) compression and (B) decompression. Pressure dependence of three characteristic Raman peaks during (C) compression and (B) decompression.

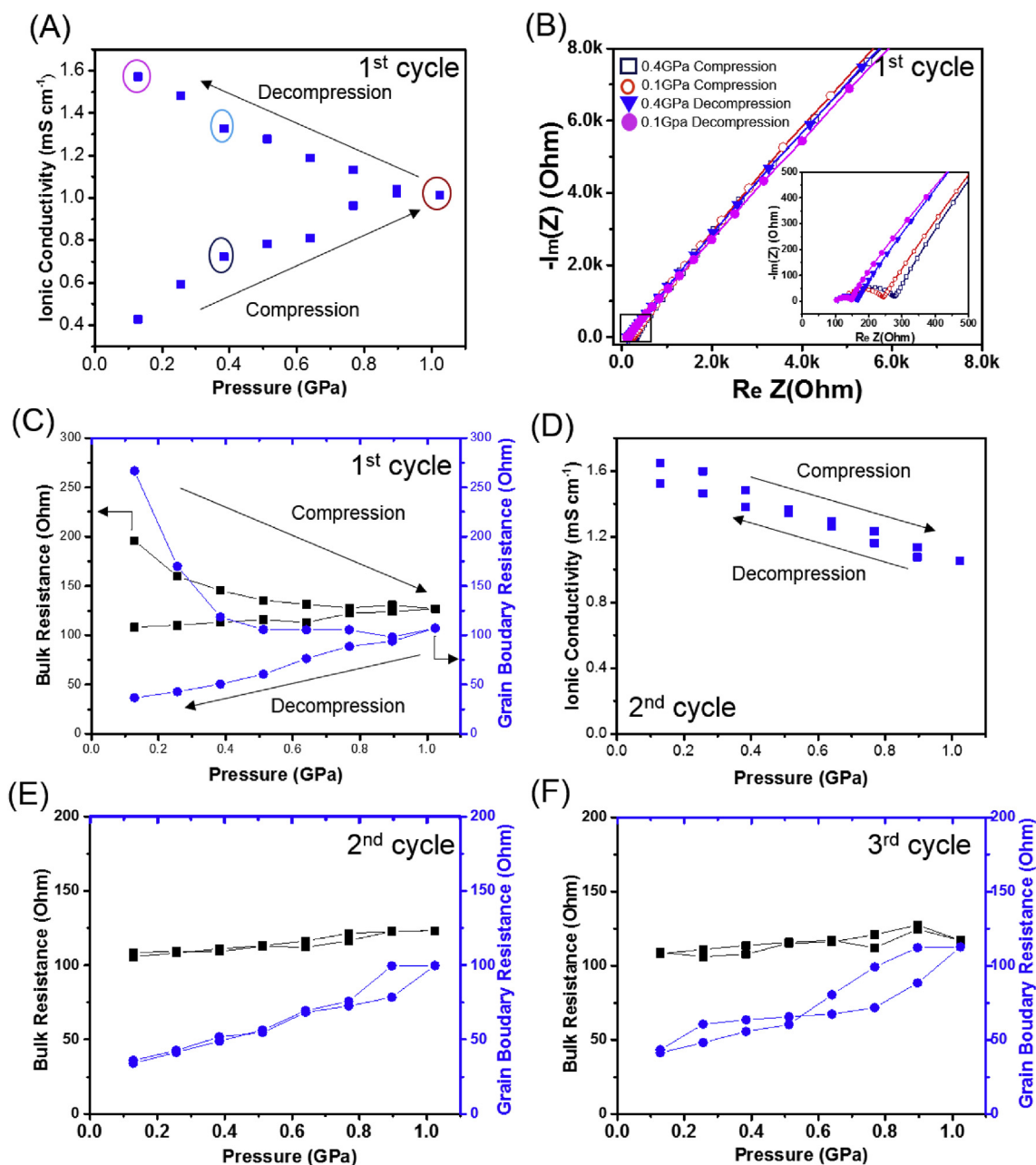


Fig. 4. (A) Pressure effect on ionic conductivities of Na₃SbS₄ during 1st cycle of compression and decompression, (B) Nyquist plots of Na₃SbS₄ solid electrolytes at 0.4 GPa and 1.1 GPa (compression), 0.4 GPa and 0.1 GPa (decompression), insert is the magnified plots. (C) pressure-dependence of bulk resistance and grain boundary resistance during 1st cycle of compression and decompression, (D) ionic conductivity of pressure-treated Na₃SbS₄ during repeated 2nd cycle for compression and decompression. The pressure effect on bulk resistance and grain boundary resistance of Na₃SbS₄ during (E) 2nd cycle and (F) 3rd cycle compression and decompression.

resistance from blocking electrode. The impedance plots are fitted by Z-fit to determine the bulk resistance (R_b) and grain boundary resistance (R_{gb}) as a function of pressure. During the 1st compression process (Fig. 4C), in addition to the obvious drop of grain boundary resistance, the bulk resistance also slightly decreases. Meanwhile, Na₃SbS₄ solid conductor is observed to densification as pressure loading (Figure S2) and the density increases to 2.72 g/cm³ (about 98% of relative density) at 1 GPa. After pressure is unloaded, the ionic conductivity of Na₃SbS₄ continues to increase, which is contributed by the decrease of grain boundary resistance. When pressure is drop down to 0.1 GPa, the ionic conductivity of Na₃SbS₄ rises to 1.6 mS cm⁻¹. The compression-decompression process was repeated for the second cycle (Fig. 4D) and the third cycle after few hours (Figure S3). Both cycles show similar trend,

in which loading pressure results in the conductivity decreases while releasing pressure leads to the increase of ionic conductivity. For the 2nd and 3rd rounds of compression/decompression (Fig. 4E and F), the pressure dependence of ionic conductivities for Na₃SbS₄ is originated from the change of grain boundary resistance in contract to the constant bulk resistance. There is almost no density change in the 2nd cycle of compression (Figure S2). After the pressure was released to 0.1 GPa, the impedance spectra were collected after holding different time (Figure S4). The ionic conductivity was found to be stable at around 1.6 mS cm⁻¹, no obvious further change was observed after 24 h.

The observation of increased ionic conductivity for Na₃SbS₄ is considered to relate with pressure treatment. Pressure had been previously reported to enhance both chemical and physical properties of

materials [41–44], but mostly resulted from phase transition. For example, black phosphorous (BP), the product of white phosphorous under high pressure, was reported to show a graphite-like layer structure and had attracted great attention as an anode material for Li-ion batteries [41]. In some cases, even the phase transitions are reversible after decompression, the pressure-driven improved material properties are still kept. It was reported that pressure-treated TiO₂ showed a significant enhancement in the electron transport properties compared with the pristine sample [42]. However, the pressure-induced conductivity increase of Na₃SbS₄ is a different case, because there is no phase transition observed when pressure is loaded. Both *in-situ* synchrotron XRD (Fig. 2) and Raman (Fig. 3) results clearly confirmed that Na₃SbS₄ keeps tetragonal phase stable during compression and decompression. In fact, the electrochemical impedance analysis (Fig. 4C, E and F) reveals that the improved conductivity of Na₃SbS₄ is resulted from the decrease of grain resistance after pressure treatment instead of bulk resistance. That observation is similar with high pressure-treated yttrium-doped SrZrO₃ [45], in which ions diffusion become easier through the boundaries. This intriguing phenomenon can be beneficial for the development of pressure as an effective tool to improve the ionic conductivities of solid electrolytes, but need further systematically investigation.

4. Conclusion

In conclusion, we have studied the structural stability and ionic conductivity of Na₃SbS₄ under pressure. MD simulation predicted that tetragonal structure of Na₃SbS₄ is more stable than cubic structure under pressure, which is further confirmed by *in-situ* XRD and Raman results. Na₃SbS₄ tetragonal structure shows anisotropic compressibility along *a* and *c* directions, with *a* axis is more compressible and increased tetragonal distortion in framework. The ionic conductivity of Na₃SbS₄ increases as pressure loading, mainly attribute to the decrease of grain boundary resistance. Interestingly, the conductivity further increases during decompression as result of the decrease of both bulk resistance and grain boundary resistance. This work demonstrates that pressure could be an effective tool to treat sulfide-based solid electrolytes to further increase their ionic conductivities.

Acknowledgement

H. Wang would like to thank the support from NSF EPSCoR Grant (1355438), Conn Center for Renewable Energy Research and EVPRI Internal Grant at University of Louisville for this work. M. Yu acknowledge computing resource support from the Cardinal Research Cluster at the University of Louisville. Z. Feng thanks the Callahan Faculty Scholar Endowment Fund from Oregon State University. The use of Advanced Photon Source (APS) of Argonne National Laboratory (ANL) is supported by Department of Energy under Contract Number DE-AC02-06CH11357. The authors also thank Dr. Zach Hood from Massachusetts Institute of Technology and Dr. Yan Chen from Oak Ridge National Laboratory for the helpful discussion.

Appendix A. Supplementary data

Supplementary data related to this article can be found at <https://doi.org/10.1016/j.jpowsour.2018.05.037>.

References

- [1] R. Kanno, M. Murayama, J. Electrochem. Soc. 148 (2001) A742–A746.
- [2] D.Y. Oh, Y.E. Choi, D.H. Kim, Y.-G. Lee, B.-S. Kim, J. Park, H. Sohn, Y.S. Jung, J. Mater. Chem. 4 (2016) 10329–10335.
- [3] F. Mizuno, A. Hayashi, K. Tadanaga, M. Tatsumisago, Adv. Mater. 17 (2005) 918–921.
- [4] N. Kamaya, K. Homma, Y. Yamakawa, M. Hirayama, R. Kanno, M. Yonemura, T. Kamiyama, Y. Kato, S. Hama, K. Kawamoto, A. Mitsui, Nat. Mater. 10 (2011) 682–686.
- [5] B.R. Shin, Y.J. Nam, D.Y. Oh, D.H. Kim, J.W. Kim, Y.S. Jung, Electrochim. Acta 146 (2014) 395–402.
- [6] O. Kwon, M. Hirayama, K. Suzuki, Y. Kato, T. Saito, M. Yonemura, T. Kamiyama, R. Kanno, J. Mater. Chem. 3 (2015) 438–446.
- [7] A. Hayashi, K. Minami, S. Ujiie, M. Tatsumisago, J. Non-Cryst. Solids 356 (2010) 2670–2673.
- [8] I.H. Chu, H. Nguyen, S. Hy, Y.C. Lin, Z. Wang, Z. Xu, Z. Deng, Y.S. Meng, S.P. Ong, ACS Appl. Mater. Interfaces 8 (2016) 7843–7853.
- [9] Z. Liu, W. Fu, E. Payzant, X. Yu, Z. Wu, N. Dudney, J. Kiggans, K. Hong, A. Rondinone, C. Liang, J. Am. Chem. Soc. 135 (2013) 975–978.
- [10] Y. Chen, L. Cai, Z. Liu, C.R. dela Cruz, C. Liang, K. An, Appl. Phys. Lett. 107 (2015).
- [11] A. Hayashi, K. Noi, N. Tanibata, M. Nagao, M. Tatsumisago, J. Power Sources 258 (2014) 420–423.
- [12] I.-H. Chu, C.S. Kompella, H. Nguyen, Z. Zhu, S. Hy, Z. Deng, Y.S. Meng, S.P. Ong, Sci. Rep. 6 (2016) 33733.
- [13] N. Tanibata, M. Deguchi, A. Hayashi, M. Tatsumisago, Chem. Mater. 29 (2017) 5232–5238.
- [14] H. Wang, Y. Chen, Z.D. Hood, G. Sahu, A.S. Pandian, J.K. Keum, K. An, C. Liang, Angew. Chem. Int. Ed. Engl. 55 (2016) 8551–8555.
- [15] L. Zhang, D. Zhang, K. Yang, X. Yan, L. Wang, J. Mi, B. Xu, Y. Li, Adv. Sci. 3 (2016) 1600089.
- [16] A. Hayashi, K. Noi, A. Sakuda, M. Tatsumisago, Nat. Commun. 3 (2012) 856.
- [17] K.Y.M. Homma, M. Nagao, R. Kanno, J. Phys. Soc. Jpn. 79 (2010) 90–93.
- [18] A. Hayashi, H. Muramatsu, T. Ohtomo, S. Hama, M. Tatsumisago, J. Mater. Chem. 1 (2013).
- [19] L.L. Baranowski, C.M. Heveran, V.L. Ferguson, C.R. Stoldt, ACS Appl. Mater. Interfaces 8 (2016) 29573–29579.
- [20] A. Sakuda, A. Hayashi, M. Tatsumisago, Sci. Rep. 3 (2013) 2261.
- [21] X.-R. Chen, X.-F. Li, L.-C. Cai, J. Zhu, Solid State Commun. 139 (2006) 246–249.
- [22] A. Bouhemadou, R. Khenata, F. Zegrar, M. Sahnoun, H. Baltache, A.H. Reshak, Comput. Mater. Sci. 38 (2006) 263–270.
- [23] A. Grzechnik, A. Vegas, K. Syassen, I. Loa, M. Hanfland, M. Jansen, J. Solid State Chem. 154 (2000) 603–611.
- [24] B.R. Maddox, C.S. Yoo, Deepa Kasinathan, W.E. Pickett, R.T. Scalettar, Phys. Rev. B 73 (2006) 144111.
- [25] X. Lu, W. Yang, Q. Jia, H. Xu, Chem. Sci. 8 (2017) 6764–6776.
- [26] P. Bhardwaj, S. Singh, Open Chem. 10 (2012).
- [27] F. Hong, B. Yue, N. Hirao, Z. Liu, B. Chen, Sci. Rep. 7 (2017) 44078.
- [28] H. Wang, Y. Chen, Z.D. Hood, G. Sahu, A.S. Pandian, J.K. Keum, K. An, C. Liang, Angew. Chem. Int. Ed. 55 (2016) 8551–8555.
- [29] D.Z. Long Zhang, Kun Yang, Xinlin Yan, Limin Wang, Jianli Mi, Bo Xu, Yueming Li, Adv. Sci. 3 (2016) 1600089.
- [30] L.E. Rush, Z.D. Hood, N.A.W. Holzwarth, Phys. Rev. Mater. 1 (2017).
- [31] A. Banerjee, K.H. Park, J.W. Heo, Y.J. Nam, C.K. Moon, S.M. Oh, S.T. Hong, Y.S. Jung, Angew. Chem. Int. Ed. 55 (2016) 9634–9638.
- [32] P. Hohenberg, W. Kohn, Phys. Rev. B 136 (1964) B864–B871.
- [33] W. Kohn, L.J. Sham, Phys. Rev. B 140 (1965) A1133–A1138.
- [34] G. Kresse, Phys. Rev. B 54 (1996) 11169–11186.
- [35] P.E. Blöchl, Phys. Rev. B 50 (1994) 17953–17979.
- [36] J.P. Perdew, J.A. Chevary, S.H. Vosko, K.A. Jackson, M.R. Pederson, D.J. Singh, C. Fiolhais, Phys. Rev. B 46 (1992) 6671–6687.
- [37] Perdew, K. Burke, M. Ernzerhof, Phys. Rev. Lett. 77 (1996) 3865–3868.
- [38] X. Gonze, Phys. Rev. B 55 (1997) 10337–10354.
- [39] H.J. Monkhorst, J.D. Pack, Phys. Rev. B 13 (1976) 5188–5192.
- [40] W. Mikenda, A. Preisinger, Spectrochim. Acta Mol. Spectros 36 (1980) 365–370.
- [41] Z. Zhao, L. Liu, T. Yu, G. Yang, A. Bergara, J. Phys. Chem. C 121 (2017) 21199–21205.
- [42] X. Lu, W. Yang, Z. Quan, T. Lin, L. Bai, L. Wang, F. Huang, Y. Zhao, J. Am. Chem. Soc. 136 (2014) 419–426.
- [43] V.V. Sinityn, J. Mater. Chem. 20 (2010).
- [44] D. Santamaria-Perez, U. Amador, J. Tortajada, R. Dominko, M.E. Arroyo-de Dompablo, Inorg. Chem. 51 (2012) 5779–5786.
- [45] L. Dai, L. Wu, H. Li, H. Hu, Y. Zhuang, K. Liu, J. Phys. Condens. Matter 28 (2016) 475501.